Extreme g-Tensor Anisotropy and Its Insensitivity to Structural Distortions in a Family of Linear Two-Coordinate Ni(I) Bis-N-heterocyclic Carbene Complexes

William J. M. Blackaby, Katie L. M. Harriman, Samuel M. Greer, Andrea Folli, Stephen Hill, Vera Krewald, Mary F. Mahon, Damien M. Murphy, Muralee Murugesu, Emma Richards,* Elizaveta Suturina,* and Michael K. Whittlesey

Read Online

ACCESS | Metrics & More | Article Recommendations | Supporting Information

ABSTRACT: We report a new series of homoleptic Ni(I) bis-N-heterocyclic carbene complexes with a range of torsion angles between the two ligands from 68° to 90°. Electron paramagnetic resonance measurements revealed a strongly anisotropic **g**-tensor in all complexes with a small variation in $g_\parallel \sim 5.7-5.9$ and $g_\perp \sim 0.6$. The energy of the first excited state identified by variable-field far-infrared magnetic spectroscopy and SOC-CASSCF/NEVPT2 calculations is in the range $270-650$ cm^{-1}. Magnetic relaxation measured by alternating current susceptibility up to 10 K is dominated by Raman and direct processes. *Ab initio* ligand-field analysis reveals that a torsion angle of <90° causes the splitting between doubly occupied d_{xz} and d_{yz} orbitals, which has little effect on the magnetic properties, while the temperature dependence of the magnetic relaxation appears to have no correlation with the torsion angle.
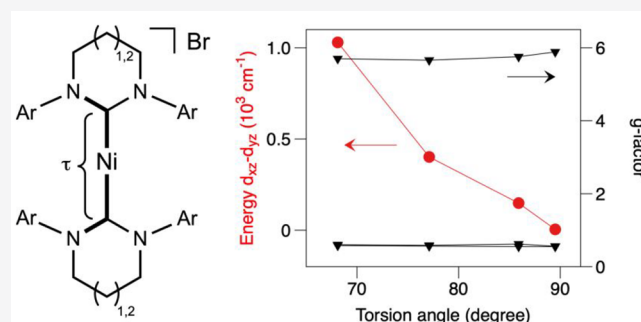
INTRODUCTION

Understanding magneto-structural correlations in transition metal complexes is one of the key aspects in the rational design of magnetic materials.[1] In particular, the connection between magnetic anisotropy and the structure of coordination compounds has attracted a great deal of attention, as it is linked to slow relaxation of the magnetization.[2−6]

The anisotropy of the magnetic properties at very low temperature is characterized by the effective **g**-tensor of the ground magnetic sublevels. At increased temperatures, other magnetic sublevels become populated, which affects the overall magnetic properties. The energy separation between magnetic sublevels at zero magnetic field is called zero-field splitting (ZFS), another important characteristic of magnetic anisotropy. Both ZFS and **g**-tensor anisotropy result from spin–orbit coupling (SOC), which is most pronounced when the orbital momentum is unquenched and the SOC constant is large. An unquenched orbital momentum is retained by a high symmetry of the first coordination sphere that leaves orbitals with unpaired electron(s) degenerate. For this reason, linear two-coordinate transition metal complexes (MX$_2$) are particularly interesting.[2,7,8]

There are several reported examples of transition metal MX$_2$ complexes exhibiting slow magnetic relaxation. Metal complexes with a 3d^7 electronic configuration, such as those of

cobalt(II)[9] and iron(I),[10−12] have the largest magnetic anisotropy and the slowest relaxation of the magnetization.

A cobalt(II) dialkyl complex reported by Bunting et al.[9] has the maximum possible contribution of the orbital momentum $|M_L| = 3$ due to a non-Aufbau electronic configuration (d$_{xy}$, d$_{x^2-y^2}$)^3(d$_{xz}$, d$_{yz}$)^3(d$_{z^2}$)^1. This leads to a doubly degenerate $^4\Phi$ ground state ($C_{\infty v}$ point group notation), which due to SOC splits into four Kramers doublets (KD) with M_J values of $\pm^9/_2$, $\pm^7/_2$, $\pm^5/_2$, and $\pm^3/_2$. The ground KD with an M_J of $\pm^9/_2$ has a theoretical limit for the effective **g**-tensor of (0, 0, 12). A recently reported study of a cobalt(II) amido complex also shows a non-Aufbau ground state; however, it has π-antibonding interactions due to amido lone pair that causes a splitting of (d$_{xz}$, d$_{yz}$) orbitals and quenches orbital momentum reducing the overall magnetic anisotropy.[13]

The electronic structure of an iron(I) dialkyl complex reported by Zadrozny et al.[10] differs from that of the cobalt(II) analogue because the low oxidation state allows for a more
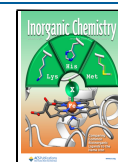
pronounced 3d−4s mixing that stabilizes the d_{z^2} orbital, leading to a $(d_{z^2})^2(d_{xy}, d_{x^2-y^2})^3(d_{xz}, d_{yz})^2$ electronic configuration. This assignment was confirmed by multipole analysis of the X-ray diffraction data.[14] This means that the orbital contribution is smaller ($|M_L| = 2$) and the ground state $^4\Delta$ splits into four KDs with M_J values of $\pm^7/_2$, $\pm^5/_2$, $\pm^3/_2$, and $\pm^1/_2$. The theoretical limit of the $M_J = \pm^7/_2$ effective **g**-tensor is (0, 0, 10). An iron(I) bis-amido complex reported by Werncke et al.[11] has a similar ordering of d orbitals; however, the anisotropy of metal−ligand π-antibonding interaction splits the (d_{xz}, d_{yz}) orbital pair.[15] This is also observed in another recently reported iron(I) bis-amido complex.[13] However, orbital splitting does not quench orbital momentum in those complexes. In contrast, an iron(I) bis-carbene complex reported by Samuel et al.[12] features anisotropy of the metal−ligand π interaction that decreases the effective anisotropy of the **g**-tensor.

Complexes with a 3d^8 configuration, in particular iron(II), were among the first MX$_2$ complexes reported to show slow magnetic relaxation, and their electronic structure and magnetic anisotropy have been studied thoroughly.[16−19] It was shown by *ab initio* analysis that changes in the ligand environment have little effect on the $^5\Delta$ ground state as the orbital contribution $|M_L| = 2$ remains largely unquenched in all cases.[20]

In the case of cobalt(I) bis-N-heterocyclic carbene (NHC) complexes, a strong correlation between the ZFS parameters and the interligand torsion angle has been reported.[21] In that study, only one of the three carbene ligands leads to an observation of the slow relaxation of the magnetization.

In this work, we focus on nickel(I) bis-NHC complexes, i.e., a 3d^9 configuration, where only one example has been published previously by some of us.[22] We now report a detailed analysis of the static and dynamic magnetic properties and electronic structures of three new nickel(I) bis-NHC complexes with a wide range of interligand torsion angles.

■ METHODS

Synthesis and General Procedures. All manipulations were carried out using standard Schlenk line, high-vacuum, and glovebox techniques. Solvents were purified using an MBraun SPS solvent system (hexane, pentane, diethyl ether, toluene, and dichloromethane) or distilled from sodium benzophenone ketyl (benzene and THF) before being sparged with argon and stored over regenerated molecular sieves. C_6D_6 and CD_2Cl_2 were vacuum transferred from K and CaH$_2$, respectively. NMR spectra were recorded at 298 K on Bruker Avance 400 and 500 MHz NMR spectrometers and referenced to solvent signals: benzene (^{1}H, δ 7.16; ^{13}C{^{1}H}, δ 128.1) and dichloromethane (^{1}H, δ 5.32; ^{13}C{^{1}H}, δ 53.8). Elemental analyses were performed by Elemental Microanalysis Analytical Services, Okehampton, Devon, U.K. Ni(COD)$_2$ (Strem) and Ni(PPh$_3$)$_2$Br$_2$ (Sigma) were used as received. **2−6Mes** was prepared as previously reported.[22]

Ni(6Xyl)(PPh$_3$)Br (1−6Xyl). 6Xyl (300 mg, 1.03 mmol),[23] Ni(COD)$_2$ (141 mg, 0.51 mmol), and Ni(PPh$_3$)$_2$Br$_2$ (381 mg, 0.51 mmol) were combined in THF and stirred for 1 h in a J. Young's ampule fitted with a PTFE tap. The resulting yellow solution was reduced to dryness, washed with Et$_2$O (2 × 10 mL), and recrystallized from THF/hexane. Yield: 530 mg (71%). ^{1}H NMR (C$_6$D$_6$, 500 MHz): δ 29.4 (br s), 16.4 (br s), 10.8 (s), 9.8 (br s), 8.5 (br s), 8.1 (br s), 2.2 (br s), 1.9 (br s), 0.7 (br s), −1.1 (br s), −17.1 (v br s). Anal. Calcd (found) for C$_{38}$H$_{39}$N$_2$PNiBr (%): C, 65.83 (65.50); H, 5.67 (5.50); N, 4.04 (4.05). Solution magnetic moment (Evans method): 2.0 μB in benzene at 298 K. The molecular structure is shown in Figure S1.

Ni(7Mes)(PPh$_3$)Br (1−7Mes). As described for **1−6Xyl**, but using 7Mes (100 mg, 0.30 mmol),[23] Ni(COD)$_2$ (41 mg, 0.15 mmol), and Ni(PPh$_3$)$_2$Br$_2$ (111 mg, 0.15 mmol). Yield: 148 mg (67%). ^{1}H NMR (C$_6$D$_6$, 500 MHz): δ 12.3 (br s), 10.6 (br s), 9.9 (br s), 8.6 (br s), 8.1 (br s), 4.5 (s), 3.3 (br s), 2.9 (m), 2.8 (s), 2.5 (s), 2.4 (br s), 1.8 (v br s), 0.9 (br s), −1.3 (br s). Anal. Calcd (found) for C$_{41}$H$_{45}$N$_2$PNiBr (%): C, 66.96 (67.22); H, 6.17 (6.26); N, 3.81 (3.41). Solution magnetic moment (Evans method): 1.8 μB in benzene at 298 K.

Ni(7Xyl)(PPh$_3$)Br (1−7Xyl). As described for **1−6Xyl**, but using 7Xyl (250 mg, 0.82 mmol),[23] Ni(COD)$_2$ (112 mg, 0.41 mmol), and Ni(PPh$_3$)$_2$Br$_2$ (303 mg, 0.41 mmol). The analytically pure product was achieved by recrystallization from C$_6$H$_6$/hexane. Yield: 377 mg (65%). ^{1}H NMR (C$_6$D$_6$, 500 MHz): δ 11.7 (br s), 10.6 (br s), 10.1 (br s), 8.5 (br s), 7.9 (br s), 3.4 (br s), 2.8 (s), 2.4−2.3 (br m), 0.9 (br s), −1.2 (br s). Anal. Calcd (found) for C$_{39}$H$_{41}$N$_2$PNiBr·0.5C$_6$H$_6$ (%): C, 67.59 (67.80); H, 5.94 (5.76); N, 3.75 (3.61). Solution magnetic moment (Evans method): 1.9 μB in benzene at 298 K. The molecular structure is shown in Figure S1.

[Ni(6Xyl)$_2$]Br (2−6Xyl). A flame-dried Schlenk flask was charged with **1−6Xyl** (96 mg, 0.14 mmol) and 6Xyl (64 mg, 0.22 mmol) in THF (30 mL), and the mixture stirred for 16 h to form an off-white suspension. The precipitate was isolated by cannula filtration, washed with Et$_2$O (2 × 10 mL), and dried under reduced pressure. Recrystallization from CH$_2$Cl$_2$/hexane yielded an off-white product. Yield: 54 mg (54%). ^{1}H NMR (CD$_2$Cl$_2$, 500 MHz): δ 54.3 (br s, 4H), 52.1 (br s, 8H), −13.3 (br s, 24H), −15.6 (s, 4H), −21.2 (s, 8H). Anal. Calcd (found) for C$_{40}$H$_{48}$N$_4$NiBr (%): C, 66.41 (66.62); H, 6.69 (6.70); N, 7.74 (7.54). Solution magnetic moment (Evans method): 3.3 μB in dichloromethane at 298 K.

[Ni(7Mes)$_2$]Br (2−7Mes). As described for **2−6Xyl**, but using **1−7Mes** (200 mg, 0.34 mmol) and 7Mes (171 mg, 0.51 mmol). Yield: 181 mg (66%). ^{1}H NMR (CD$_2$Cl$_2$, 500 MHz, 298 K): δ 49.2 (br s, 8H), 38.7 (br s, 8H), −8.3 (s, 12H), −11.2 (br s, 24H), −17.7 (s, 8H). Despite multiple recrystallizations, efforts to determine accurate elemental analyses repeatedly gave a low %C value. Anal. Calcd (found) for C$_{46}$H$_{60}$N$_4$NiBr (%): C, 68.41 (67.43); H, 7.49 (7.51); N, 6.93 (6.82). Solution magnetic moment (Evans method): 3.0 μB in dichloromethane at 298 K.

[Ni(7Xyl)$_2$]Br (2−7Xyl). As described for **2−6Xyl**, but using **1−7Xyl** (200 mg, 0.35 mmol) and 7Xyl (162 mg, 0.53 mmol). Yield: 205 mg (77%). ^{1}H NMR (CD$_2$Cl$_2$, 500 MHz): δ 51.1 (br s, 8H), 40.0 (br s, 8H), −11.8 (br s, 24H), −14.1 (s, 4H), −18.2 (s, 8H). Anal. Calcd (found) for C$_{42}$H$_{52}$N$_4$NiBr (%): C, 67.13 (67.39); H, 6.97 (6.82); N, 7.46 (7.31). Solution magnetic moment (Evans method): 3.1 μB in dichloromethane at 298 K.

SQUID Magnetometry. Magnetic susceptibility measurements were taken using a Quantum Design SQUID magnetometer (MPMS-XL7) operating between 1.8 and 300 K. Direct current (dc) measurements were performed on polycrystalline samples of 26, 27, and 26 mg for **2−6Xyl**, **2−7Mes**, and **2−7Xyl**, respectively. The samples were prepared under an inert atmosphere in an MBraun glovebox and wrapped in a polyethylene membrane. The samples were subjected to dc fields of ≤7 T, and a 3.78 Oe driving field was used for alternating current (ac) measurements. The magnetization data were collected at 100 K to check for ferromagnetic impurities, which were absent in all samples. Diamagnetic corrections were applied for the sample holder.

Electron Paramagnetic Resonance (EPR). Samples for EPR measurements were prepared under a N$_2$ atmosphere in a glovebox. A solution of each complex was prepared by dissolving ~4 mg of **2−6Xyl, 7Mes, 6Mes,** or **7Xyl** in 100 μL of dry CH$_2$Cl$_2$. The solutions were transferred to an EPR tube, sealed in the glovebox, and then cooled to 77 K before being rapidly transferred to the precooled EPR cavity. The X-band CW EPR measurements were performed on a Bruker EMX spectrometer utilizing an ER 072 magnet/ER 081 power supply combination (maximum field of 0.6 T) and an ER4119HS resonator, operating at 100 kHz field modulation and 10 mW microwave power at 140 K. Additional EPR measurements were performed on a Bruker E500 spectrometer equipped with an Oxford Instruments liquid-helium cryostat utilizing an ER 073 magnet/ER

083 power supply combination (maximum field of 1.45 T) and an ER4102ST resonator, operating at 100 kHz field modulation and 0.63 mW microwave power at 10 K.

High-frequency Electron Paramagnetic Resonance spectra were recorded on microcrystalline powder samples contained in a polyethylene cup. The transmission-type spectrometer used in this study employed a 17 T superconducting magnet.[24] Microwave frequencies were generated in the range of 52−314 GHz using a phase-locked Virginia Diodes source combined with a series of frequency multipliers. The field-modulated signal was detected by an InSb hot-electron bolometer (QMC Ltd., Cardiff, U.K.). Temperature control was realized using an Oxford Instruments (Oxford, U.K.) continuous-flow cryostat. Angle-dependent spectra of single crystals of **2-NHC** were recorded at 16.77 GHz using a high-sensitivity cavity perturbation technique. For this measurement, the microwaves were generated and detected by a millimeter-wave vector network analyzer (MVNA), the details of which have been described elsewhere.[25,26] The magnetic field and cryostat assembly are those associated with a Quantum Design Physical Property Measurement System (PPMS). One alteration from the typical PPMS design was that the 7 T superconducting magnet was oriented horizontal relative to the sample chamber. This split solenoid, vertical-bore magnet thus facilitates in situ rotation of the cavity relative to the applied field. Once the field was aligned parallel to the hard plane, spectra were recorded at multiple frequencies for a reliable determination of the effective g-value.

Far-Infrared (far-IR) Magnetic Spectroscopy (FIRMS). Far-IR spectra were recorded using a Bruker Vertex 80v vacuum FTIR spectrometer with a resolution of 0.12 cm^{-1} at 4.2 K, over a range of 7−1000 cm^{-1}. The transmitted IR radiation was detected using a composite Si bolometer placed directly beneath the sample. The sample was mounted such that the applied field was parallel to the direction of light propagation (Faraday geometry).[27] Four spectra were recorded at each field between 0 and 17 T in 1 T increments. To differentiate the magnetic from nonmagnetic transitions, each spectrum was divided by a reference spectrum. This procedure was done for multiple choices of reference, all of which furnish final spectra with consistent field-dependent behavior. The divided spectra in the text were prepared by using the spectrum recorded at a 4 T higher applied field as the reference.

Ab Initio Calculations. Starting from the X-ray crystal structures, we performed geometry optimizations with ORCA[28,29] by relaxing only the H atom positions or the full molecule. The density functional chosen was BP86 together with dispersion corrections with Becke−Johnson damping and zeroth-order relativistic corrections, including the one-center approximation. The scalar-relativistically recontracted ZORA-def2-TZVP basis set was used on all atoms except C and H, for which ZORA-def2-SVP was used.[30,31] To accelerate the calculations, the resolution of the identity (RI) approximation was invoked together with the SARC/J auxiliary basis. The grid and integration accuracy were both increased to 7 in ORCA nomenclature. Tight SCF and geometry convergence criteria were used.

CASSCF and strongly contracted NEVPT2 calculations including spin−orbit coupling were performed using a def2-TZVP basis set on all atoms and def2-TZVP/C auxiliary basis sets due to the use of the RI approximation. The active space was defined as nine electrons in five orbitals. Five roots with a multiplicity of 2 were calculated. On the basis of this wave function, the g-tensor, susceptibility, and magnetization were calculated. Ab initio ligand-field analysis was employed to extract the energies and composition of the d orbitals.[32]

■ RESULTS AND DISCUSSION

The synthesis of the new complexes **2−6Xyl**, **2−7Mes**, and **2−7Xyl** (Scheme 1) involved reactions of the three-coordinate Ni(I) precursors Ni(NHC)(PPh₃)Br (**1-NHC**) (Figure S1) with an excess of the corresponding free NHC in a THF solution at room temperature. The two-coordinate products

Scheme 1. Synthesis of Two-Coordinate [Ni(NHC)₂]Br Complexes 2−6Mes (n = 1, Ar = 2,4,6-Me₃C₆H₂), 2−6Xyl (n = 1, Ar = 2,6-Me₂C₆H₃), 2−7Mes (n = 2, Ar = 2,4,6-Me₃C₆H₂), and 2−7Xyl (n = 2, Ar = 2,6-Me₂C₆H₃) with a Pronounced Variation of the Interligand Torsion Angle (τ)
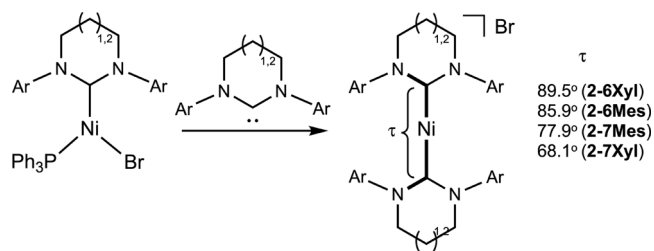
were isolated as off-white or pale-yellow solids in yields of 54−77%.

Isolation of crystals suitable for X-ray crystallography revealed linear C$_{NHC}$−Ni−C$_{NHC}$ [178.92(11)−179.78(15)°] arrangements in **2-NHC** and very little variation in Ni−C bond lengths [1.943(2)−1.959(3) Å (Figure 1)]. The crystal packing varies with the type of NHC: **2−6Xyl**, $C2/c$; **2−7Mes**, $Pca2_1$; **2−6Mes**, $P2_1$; **2−7Xyl**, $C2/c$. The shortest intermolecular Ni···Ni distances are 10.4, 10.6, 10.3, and 10.4 Å, respectively (Figure S2). The asymmetric units of **2−6Xyl** and **2−7Xyl** each contain half of a cation; the remainder is generated by virtue of a 2-fold crystallographic rotation axis in each case. There is a solvent of crystallization present, in a CH₂Cl₂:cation ratio of 2:1 for **2−6Xyl** and **2−7Xyl**, while the comparative ratio for **2−7Mes** is 1:1. The crystal structures also highlight variation in the torsion angle between the two NHCs coordinated to each nickel center. In particular, the angles between mean planes based on the metal center, ligand nitrogens, and the carbene carbon for each ligand decrease from 89.49(11)° for **2−6Xyl** to 85.82(13)° for **2−6Mes**, 77.85(11)° for **2−7Mes**, and, smallest of all, 68.08(10)° for **2−7Xyl**.

Solution magnetic moment measurements of **2-NHC** in dichloromethane (Evans method) revealed μ_{eff} values of 3.0−3.3 μ_B, which are much higher than the spin-only value of 1.73 μ_B.

SQUID measurements of the magnetic susceptibility for polycrystalline powders under a 0.1 T static field also showed χT values at 300 K in the range of 1.2−1.3 cm³ K mol^{-1} (3.1−3.2 μ_B), much higher than the theoretical spin-only value of 0.375 cm³ K mol^{-1}. With a decrease in temperature, the χT value stayed nearly constant until approximately 5 K, where it decreased sharply, suggesting a relatively weak intermolecular interaction (Figure S11). The molar magnetization measured between 1.8 and 7 K and 0 and 7 T has near-saturation values of 1.7−1.9 μ_B (Figure S11). Assuming axial anisotropy of the g-tensor, the high-temperature powder magnetic susceptibility and magnetization saturation values can be approximated as

$$\chi T = \frac{N\mu_B^2 S(S+1)}{9k}(g_\parallel^2 + 2g_\perp^2) \tag{1}$$

$$M_S = N\mu_B S\sqrt{\frac{g_\parallel^2 + 2g_\perp^2}{3}} \tag{2}$$

where N is Avogadro's number, S is the total spin, k is the Boltzmann constant, and $g_\parallel$ and $g_\perp$ are components of the g-tensor.
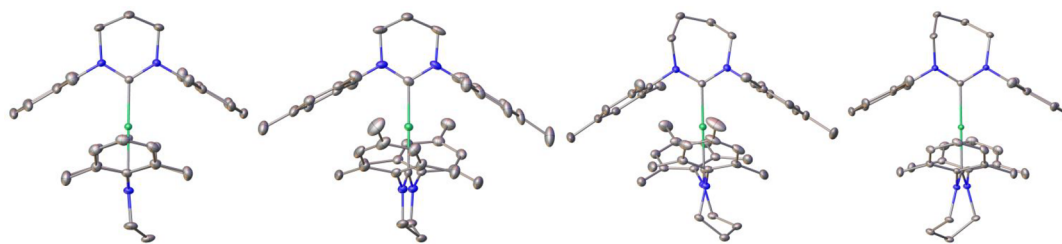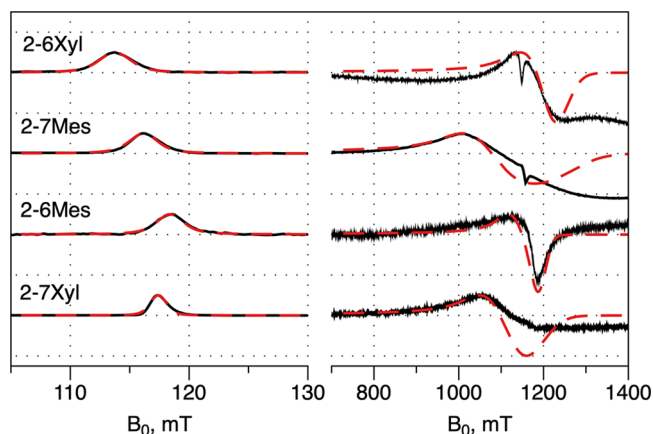
Figure 1. X-ray crystal structures of the cations in **2−6Xyl**, **2−6Mes**, **2−7Mes**, and **2−7Xyl** are shown from left to right, respectively. Color code: Ni, green; N, blue; C, gray. The minor disordered component of **2−6Mes** and hydrogen atoms have been omitted for the sake of clarity. Thermal ellipsoids are shown at the 30% probability level. The orientation is chosen so that one of the NHC planes is within the plane of the figure, highlighting the differences in the torsion angle between the two ligands.

SQUID measurements are not sufficient to identify both $g_\parallel$ and $g_\perp$ independently; nevertheless, they set limitations on the combinations of $g_\parallel$ and $g_\perp$ (Figure S12).

Solution ^{1}H NMR spectra of **2-NHC** featured five strongly paramagnetically shifted peaks in the range of −25 to 55 ppm at 298 K (Figures S6−S9). DFT calculations of the hyperfine tensors suggest that the proton paramagnetic shifts are dominated by a pseudocontact contribution (PCS). Assuming uniaxial anisotropy, the best fit for the axiality of the magnetic susceptibility tensor, $\Delta\chi_{ax}$, extracted from the PCS data at 298 K is 0.13−0.15 Å^3 (Table S2), suggesting a large anisotropy of the g-tensor with $g_\parallel^2 - g_\perp^2$ in the range of 19−22. Considering both paramagnetic NMR and SQUID constraints together, we can estimate $g_\parallel \sim 5$ and $g_\perp \sim 2$.

To determine definitively the g-values, we employed a series of high-field EPR experiments on a single crystal, as well as a polycrystalline powder of **2−6Mes** (Figure S16). These experiments revealed a remarkably anisotropic **g**-tensor: $g_\parallel =$ 5.42, and $g_\perp =$ 0.36. This observation showed that an analogous measurement at X-band (9.5 GHz) would require a magnetic field above the maximum attainable for most X-band magnets (typically <1 T). The X-band results were therefore acquired using two magnet systems (see the Supporting Information). Measurements on frozen solutions of **2-NHC** showed that the $g_\parallel$ values for all complexes are in the range of 5.7−5.9 (Figure 2 and Figure S14) and $g_\perp \sim 0.6$

(Figure 2); the differences between the solid state and solution spectra are likely due to small variations in the molecular structures. Such highly anisotropic **g**-tensors are uncommon for a 3d^9 electronic configuration. Examples of similar magnetic anisotropy in $S = \frac{1}{2}$ complexes occur in actinide and lanthanide systems[24] and some rare cases of low-spin d^5 complexes such as Os(III).[33,34]

The origin of the large magnetic anisotropy in **2-NHC** was unveiled by *ab initio* ligand-field analysis (AI LFT) based on CASSCF(9,5)/NEVPT2 calculations (Figure 3).
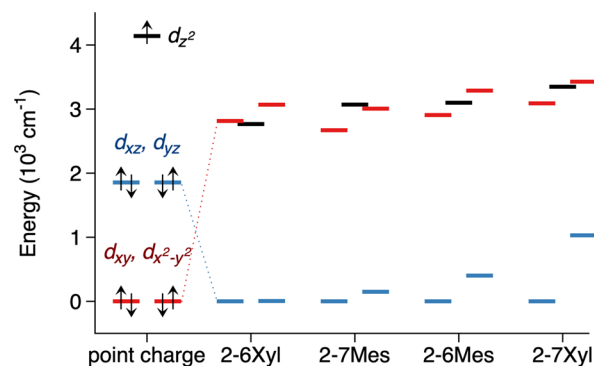
Figure 3. Ligand-field splitting of d orbitals expected for a linear two-coordinate system with point charges in comparison with the ligand-field splitting in **2-NHC** calculated using AI LFT based on CASSCF(9,5)/NEVPT2/def2-TZVP (see also Figure S18 for AI LFT orbitals).

Following a simple crystal-field model, one would expect that the energetic ordering of the d orbitals in a linear two-coordinate complex would be $(d_{xy}, d_{x^2-y^2}) < (d_{xz}, d_{yz}) < d_{z^2}$.[35] Hence, a d^9 configuration should yield an orbitally non-degenerate ground state $^2\Sigma^-$ with an almost isotropic **g**-tensor. Indeed, this is what is observed in the formally isoelectronic Cu(II) bis-amido complexes.[36] However, the AI LFT (Figure 3) suggests that the order of d orbitals in **2-NHC** is completely different: $(d_{xz}, d_{yz}) < d_{z^2} \approx (d_{xy}, d_{x^2-y^2})$. The (d_{xz}, d_{yz}) orbital pair is stabilized due to strong π-back bonding from the NHC ligands, while the d_{z^2} orbital is stabilized by 3d−4s mixing. Both effects make the $(d_{xy}, d_{x^2-y^2})$ orbital pair that carries the largest orbital momentum projection $|M_L| = 2$ highest in energy, creating an orbitally degenerate ground state $^2\Delta$ with a very large **g**-tensor anisotropy (Table 1). The theoretical maximum for **g**-tensor anisotropy according to ligand-field theory is (0, 0, 6), which is almost achieved in **2-NHC**.

Variation of the torsion angle between ligands across the series primarily affects the splitting of the (d_{xz}, d_{yz}) orbitals.
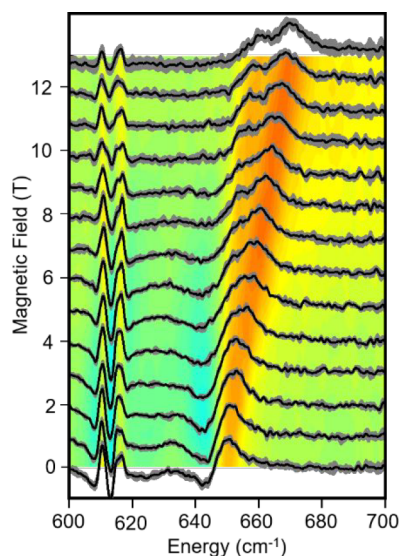

Figure 2. Continuous-wave X-band EPR spectra of frozen CH$_2$Cl$_2$ solutions of **2-NHC** measured at 10 K up to 130 mT (Bruker EMX, 8 in. magnet) and from 700 to 1400 mT (Bruker E500, 10 in. magnet). The microwave frequencies from top to bottom are 9.3820, 9.3814, 9.3926, and 9.3928 GHz, respectively, plotted normalized to 9.5 GHz. The red lines show EasySpin simulations with the parameters listed in Table 1.

Table 1. Experimental and *Ab Initio*-Calculated [shown in parentheses, CASSCF(9,5)/NEVPT2/def2-TZVP] g-Tensors of 2-NHC

	g_1	g_2	g_3
2−6Xyl	0.55 (0.53)	0.56 (0.53)	5.887 (5.89)
2−7Mes	0.55 (0.60)	0.62 (0.66)	5.755 (5.77)
2−6Mes	0.565 (0.72)	0.585 (0.74)	5.66 (5.77)
2−7Xyl	0.58 (0.64)	0.602 (0.66)	5.70 (5.81)

They are degenerate when $\angle$N−C−C−N = 90° (**2−6Xyl**), and their splitting increases as the torsion angle decreases (Figure 3). However, both orbitals (d_{xz}, d_{yz}) are doubly occupied, and their energy splitting does not significantly affect the magnetic properties. The splitting of (d_{xy}, $d_{x^2-y^2}$) and the relative position of d_{z^2} are much more important for the **g**-tensor anisotropy of **2-NHC**.

Such variation of the torsion angle in linear two-coordinate metal(I) bis-carbene complexes is expected to affect the magnetic properties of a $3d^6$ configuration [e.g., Mn(I)], where an odd number of electrons occupy the (d_{xz}, d_{yz}) orbitals, but the only example of such a complex for manganese is [Mn(cAAC)$_2$], which features Mn(II) and radical ligands.[37] Linear Fe(I) bis-carbene complexes may also be affected by ligand rotation if the highest-energy (d_{xz}, d_{yz}) orbitals become degenerate with (d_{xy}, $d_{x^2-y^2}$) at a torsion angle of 0°, which seems to be the case for [Fe(cAAC)]$^+$, as it was reported to have a large effective magnetic moment $\mu_{\text{eff}} \sim 5\ \mu_B$ (the spin-only value is 3.8 μ_B) and slow magnetic relaxation.[12]

The separation between the ground doublet and the first excited doublet in **2−6Mes** was measured by variable-field FIRMS spectroscopy to be $\sim$643 cm^{-1} (Figure 4 and Figure S17). *Ab initio* results for the SOC-corrected first excited doublet state show some variation within the series: 653 cm^{-1}

for **2−6Xyl**, 277 cm^{-1} for **2−7Mes**, 514 cm^{-1} for **2−6Mes**, and 407 cm^{-1} for **2−7Xyl**. There appears to be no correlation between the relative orientation of the two carbene ligands and the predicted energy gap as more subtle nonbonding interactions with the *N*-aryl substituents of the ligands are responsible for splitting and mixing of $d_{x^2-y^2}$, d_{xy}, and d_{z^2} orbitals. A simple ligand-field model suggests that the effects of SOC on a degenerate d_{xy} and $d_{x^2-y^2}$ orbital pair will produce two Kramers doublets ($M_J = \pm^5/_2$ and $\pm^3/_2$) separated by 2ζ, where ζ is the spin−orbit coupling constant [Ni(I) $\zeta \approx 600$ cm^{-1}]. This suggests that the first spin−orbit state exists $\geq$1200 cm^{-1} above the ground state, a prediction that is incompatible with the experimentally observed gap of $\sim$643 cm^{-1} and suggests that an additional state is present. Examination of the AI LFT orbital splitting shows that the d_{z^2} orbital is similar in energy to the d_{xy} and $d_{x^2-y^2}$ orbitals and, thus, gives rise to a third low-lying Kramers doublet (Table S3). The *ab initio* calculations reveal that these orbitals are highly mixed, which makes qualitative rationalization of trends in excited state energies difficult. However, a simple ligand-field model (see the Supporting Information) considering only the effects of SOC on a degenerate d_{z^2}, d_{xy}, or $d_{x^2-y^2}$ orbital set results in three Kramers doublets, each separated by ζ ($\sim$600 cm^{-1}). This value is extremely close to the gap observed by the FIRMS experiments.

Such extraordinary magnetic anisotropy of $3d^9$ systems is the reason behind the previously observed slow relaxation of the magnetization in **2−6Mes**.[22] Even slower magnetic relaxation is recorded for **2−6Xyl** and **2−7Mes**, while **2−7Xyl** shows a marginally faster relaxation rate (Figures 5 and 6 and Figure S13).

The fit of the temperature dependence of the relaxation data was done assuming Raman and direct processes (eq 3)
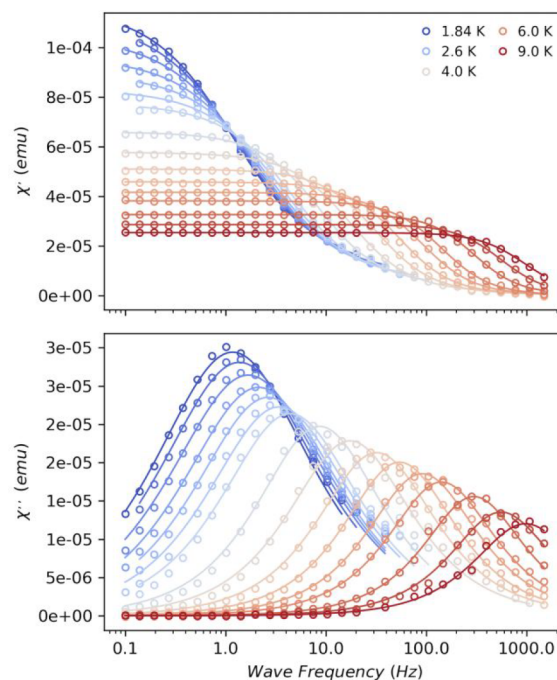

Figure 4. FIRMS spectra of **2−6Mes** divided by reference spectra recorded at a 4 T larger field. The data have been offset by the magnetic field of each recorded spectrum. The gray shading around each spectrum is the standard deviation of the four recorded spectra at each field. The bottom surface is a 2D false color plot showing the evolution of the spectral features with an applied field. A pair of features centered at $\sim$612 cm^{-1} are independent of the field, while the feature originating at $\sim$643 cm^{-1} displays a pronounced field dependence.

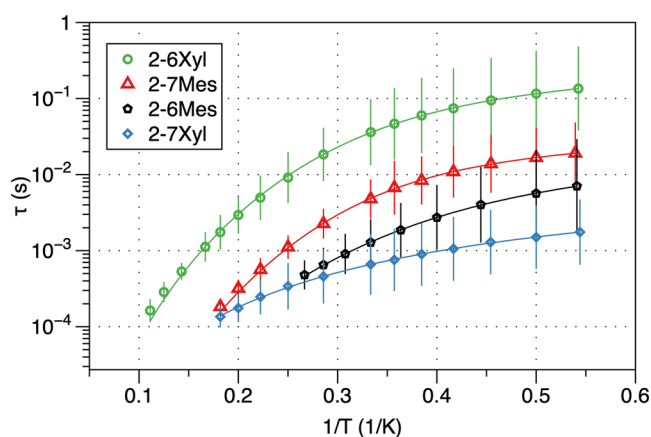**Figure 5.** In-phase (χ', top) and out-of-phase (χ'', bottom) powder magnetic susceptibility under a 600 Oe applied magnetic field of **2−6Xyl** (circles) and generalized Debye model fits (lines) obtained with CC-FIT2.[38]

Figure 6. Temperature dependence of the relaxation times obtained under a 600 Oe applied dc field extracted from ac susceptibility measurements (symbols) and fit curves (solid lines) with Raman and direct processes (see the text for details).

$$\frac{1}{\tau} = CT^n + AT \tag{3}$$

where A is the parameter for the direct process and C is the parameter for the Raman process. Inclusion of the Orbach relaxation mechanism, which relies on the presence of a thermally accessible excited state, does not lead to an improvement in the fit in the measured low-T range (<10 K). It is expected for **2-NHC**, where the first excited state is well above 200 cm^{-1} according to FIRMS and *ab initio* results.

The best-fit parameters are listed in Table 2. The constants A and C of the respective direct and Raman processes increase

Table 2. Best-Fit Parameters of the Temperature Dependence of the Relaxation Time

	C (s^{-1} K^{-n})	n	A (s^{-1} K^{-1})
2−6Xyl	0.04	5.6	3
2−7Mes	0.12	6.4	25
2−6Mes	2.1	5.2	50
2−7Xyl	28	3.2	206

from **2−6Xyl** to **2−7Xyl**. Meanwhile, the power in the Raman process, n, is smaller for **2−7Xyl** than for the rest of the series.

Despite large uncertainties in the relaxation time, there is a noticeable difference at the low-temperature limit reflected in the large variation of best-fit parameters for both direct and Raman processes (Table 2). Relaxation data were acquired without any magnetic dilution; hence, variations in dipolar couplings could be one of the reasons behind the low-temperature differences. However, **2−6Xyl** and **2−7Xyl** have very similar crystal packing and **g**-tensors; hence, dipolar coupling is expected to be essentially the same for these two compounds. Nevertheless, the low-temperature relaxation time differs the most between **2−6Xyl** and **2−7Xyl**. Available *ab initio* studies of the magnetic relaxation in transition metal complexes[39−42] point out the importance of the molecular rigidity that can control the admixture of intramolecular vibrational modes that modulate the spin-Hamiltonian parameters via acoustic phonons, thus driving low-temperature relaxation. The more rigid structure of the smaller carbene in **2−6Xyl** might therefore also contribute to its slower relaxation compared to the larger, less rigid NHC in **2−7Xyl**. Moreover, the difference in electrostatic polarization of the donor atom

may also affect Raman relaxation, as highlighted in the recent work by Lunghi et al.[43] Further studies of these Ni compounds are needed to rationalize fully the relaxation behavior. Given the very similar electronic structures, **g**-tensor anisotropy, and crystal packing, but different carbene−Ni−carbene torsion angles, **2−6Xyl** and **2−7Xyl** are excellent candidates for further *ab initio* analysis of the role of phonons in the low-temperature limit of Raman relaxation.

CONCLUSIONS

In summary, we have reported the synthesis and characterization of three new linear two-coordinate Ni(I) bis-NHC complexes with highly anisotropic **g**-tensors. We have characterized these compounds *via* a combination of advanced EPR spectroscopy, magnetometry, and paramagnetic NMR analysis. *Ab initio* studies show that **2-NHC** has an orbitally degenerate ground state $^2\Delta$ due to carbene π-back bonding and 3d−4s mixing that completely changes the d orbital splitting from that in a simple crystal-field picture to $(d_{xz}, d_{yz}) < (d_{z^2}) \approx (d_{xy}, d_{x^2-y^2})$. This leads to a very large magnetic anisotropy, $g_\parallel \sim 5.7−5.9$ and $g_\perp \sim 0.6$, as confirmed by EPR.

Contrary to expectations, the ligand rotation in the series was found to have little effect on the static magnetic properties as it mostly affects the splitting of the doubly occupied orbitals (d_{xz}, d_{yz}). There is a noticeable variation in the low-temperature magnetic relaxation profile within the series of **2−6Xyl**, **2−7Mes**, **2−6Mes**, and **2−7Xyl**; however, there is no correlation with the torsion angle. The electronic structure and crystal packing of **2−6Xyl** and **2−7Xyl** are very similar; hence, an order of magnitude difference in the low-T magnetic relaxation time could be attributed to differences in vibrational modes and spin-phonon coupling.

ASSOCIATED CONTENT

Ⓢ **Supporting Information**

The Supporting Information is available free of charge at https://pubs.acs.org/doi/10.1021/acs.inorgchem.1c02413.

> Details for X-ray diffraction data, NMR spectra, SQUID magnetometry results, EPR and FIRMS spectra, and AI LFT molecular orbitals (PDF)

Accession Codes

CCDC 2083185−2083189 contain the supplementary crystallographic data for this paper. These data can be obtained free of charge via www.ccdc.cam.ac.uk/data_request/cif, or by emailing data_request@ccdc.cam.ac.uk, or by contacting The Cambridge Crystallographic Data Centre, 12 Union Road, Cambridge CB2 1EZ, UK; fax: +44 1223 336033.

AUTHOR INFORMATION

Corresponding Authors

> **Emma Richards** − *School of Chemistry, Cardiff University, Cardiff CF10 3AT, U.K.;* Ⓞ orcid.org/0000-0001-6691-2377; Email: RichardsE10@cardiff.ac.uk
>
> **Elizaveta Suturina** − *Department of Chemistry, University of Bath, Bath BA2 7AY, U.K.;* Ⓞ orcid.org/0000-0003-4407-1882; Email: e.suturina@bath.ac.uk

Authors

> **William J. M. Blackaby** − *Department of Chemistry, University of Bath, Bath BA2 7AY, U.K.*

Katie L. M. Harriman − *Department of Chemistry and Biomolecular Sciences, University of Ottawa, Ottawa, Ontario K1N 6N5, Canada*

Samuel M. Greer − *National High Magnetic Field Laboratory, Florida State University, Tallahassee, Florida 32310, United States; Department of Chemistry, Florida State University, Tallahassee, Florida 32306, United States;* orcid.org/0000-0001-8225-3252

Andrea Folli − *School of Chemistry, Cardiff University, Cardiff CF10 3AT, U.K.;* orcid.org/0000-0001-8913-6606

Stephen Hill − *National High Magnetic Field Laboratory, Florida State University, Tallahassee, Florida 32310, United States; Department of Physics, Florida State University, Tallahassee, Florida 32306, United States;* orcid.org/0000-0001-6742-3620

Vera Krewald − *Theoretical Chemistry, TU Darmstadt, 64287 Darmstadt, Germany;* orcid.org/0000-0002-4749-4357

Mary F. Mahon − *Department of Chemistry, University of Bath, Bath BA2 7AY, U.K.*

Damien M. Murphy − *School of Chemistry, Cardiff University, Cardiff CF10 3AT, U.K.;* orcid.org/0000-0002-5941-4879

Muralee Murugesu − *Department of Chemistry and Biomolecular Sciences, University of Ottawa, Ottawa, Ontario K1N 6N5, Canada*

Michael K. Whittlesey − *Department of Chemistry, University of Bath, Bath BA2 7AY, U.K.*

Complete contact information is available at:
https://pubs.acs.org/10.1021/acs.inorgchem.1c02413

Notes
The authors declare no competing financial interest.

■ REFERENCES

(1) Coronado, E. Molecular magnetism: from chemical design to spin control in molecules, materials and devices. *Nat. Rev. Mater.* **2020**, *5* (2), 87−104.

(2) Bar, A. K.; Pichon, C.; Sutter, J.-P. Magnetic anisotropy in two- to eight-coordinated transition-metal complexes: Recent developments in molecular magnetism. *Coord. Chem. Rev.* **2016**, *308*, 346−380.

(3) Meng, Y.-S.; Jiang, S.-D.; Wang, B.-W.; Gao, S. Understanding the Magnetic Anisotropy toward Single-Ion Magnets. *Acc. Chem. Res.* **2016**, *49* (11), 2381−2389.

(4) Atanasov, M.; Aravena, D.; Suturina, E.; Bill, E.; Maganas, D.; Neese, F. First principles approach to the electronic structure, magnetic anisotropy and spin relaxation in mononuclear 3d-transition metal single molecule magnets. *Coord. Chem. Rev.* **2015**, *289−290*, 177−214.

(5) Legendre, C. M.; Damgaard-Møller, E.; Overgaard, J.; Stalke, D. The Quest for Optimal 3d Orbital Splitting in Tetrahedral Cobalt Single-Molecule Magnets Featuring Colossal Anisotropy and Hysteresis. *Eur. J. Inorg. Chem.* **2021**, *2021* (30), 3108−3114.

(6) Bone, A. N.; Widener, C. N.; Moseley, D. H.; Liu, Z.; Lu, Z.; Cheng, Y.; Daemen, L. L.; Ozerov, M.; Telser, J.; Thirunavukkuarasu, K.; Smirnov, D.; Greer, S. M.; Hill, S.; Krzystek, J.; Holldack, K.; Aliabadi, A.; Schnegg, A.; Dunbar, K. R.; Xue, Z.-L. Applying Unconventional Spectroscopies to the Single-Molecule Magnets, $Co(PPh_3)_2X_2$ (X = Cl, Br, I): Unveiling Magnetic Transitions and Spin-Phonon Coupling. *Chem. - Eur. J.* **2021**, *27* (43), 11110−11125.

(7) Layfield, R. A. Organometallic single-molecule magnets. *Organometallics* **2014**, *33* (5), 1084−1099.

(8) Feng, M.; Tong, M.-L. Single ion magnets from 3d to 5f: developments and strategies. *Chem. - Eur. J.* **2018**, *24* (30), 7574−7594.

(9) Bunting, P. C.; Atanasov, M.; Damgaard-Møller, E.; Perfetti, M.; Crassee, I.; Orlita, M.; Overgaard, J.; van Slageren, J.; Neese, F.; Long, J. R. A linear cobalt(II) complex with maximal orbital angular momentum from a non-Aufbau ground state. *Science* **2018**, *362* (6421), eaat7319.

(10) Zadrozny, J. M.; Xiao, D. J.; Atanasov, M.; Long, G. J.; Grandjean, F.; Neese, F.; Long, J. R. Magnetic blocking in a linear iron(I) complex. *Nat. Chem.* **2013**, *5*, 577−581.

(11) Werncke, C. G.; Bunting, P. C.; Duhayon, C.; Long, J. R.; Bontemps, S.; Sabo-Etienne, S. Two-coordinate iron(I) complex $[Fe\{N(SiMe_3)_2\}_2]^-$: synthesis, properties, and redox activity. *Angew. Chemie Int. Ed.* **2015**, *54* (1), 245−248.

(12) Samuel, P. P.; Mondal, K. C.; Amin Sk, N.; Roesky, H. W.; Carl, E.; Neufeld, R.; Stalke, D.; Demeshko, S.; Meyer, F.; Ungur, L.; Chibotaru, L. F.; Christian, J.; Ramachandran, V.; van Tol, J.; Dalal, N. S. Electronic structure and slow magnetic relaxation of low-coordinate cyclic alkyl(amino) carbene stabilized iron(I) complexes. *J. Am. Chem. Soc.* **2014**, *136* (34), 11964−11971.

(13) Errulat, D.; Harriman, K. L. M.; Gálico, D. A.; Ovens, J. S.; Mansikkamäki, A.; Murugesu, M. Aufbau vs. non-Aufbau ground states in two-coordinate d^7 single-molecule magnets. *Inorg. Chem. Front.* **2021**, *8*, 5076.

(14) Thomsen, M. K.; Nyvang, A.; Walsh, J. P. S.; Bunting, P. C.; Long, J. R.; Neese, F.; Atanasov, M.; Genoni, A.; Overgaard, J. Insights into Single-Molecule-Magnet Behavior from the Experimental Electron Density of Linear Two-Coordinate Iron Complexes. *Inorg. Chem.* **2019**, *58* (5), 3211−3218.

(15) Werncke, C. G.; Suturina, E.; Bunting, P. C.; Vendier, L.; Long, J. R.; Atanasov, M.; Neese, F.; Sabo-Etienne, S.; Bontemps, S. Homoleptic Two-Coordinate Silylamido Complexes of Chromium(I), Manganese(I), and Cobalt(I). *Chem. - Eur. J.* **2016**, *22* (5), 1668−1674.
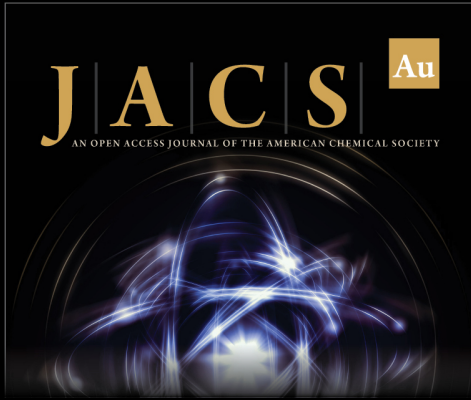
(16) Zadrozny, J. M.; Atanasov, M.; Bryan, A. M.; Lin, C.-Y.; Rekken, B. D.; Power, P. P.; Neese, F.; Long, J. R. Slow magnetization dynamics in a series of two-coordinate iron(II) complexes. *Chem. Sci.* **2013**, *4* (1), 125−138.

(17) Reiff, W. M.; LaPointe, A. M.; Witten, E. H. Virtual Free Ion Magnetism and the Absence of Jahn−Teller Distortion in a Linear Two-Coordinate Complex of High-Spin Iron(II). *J. Am. Chem. Soc.* **2004**, *126* (33), 10206−10207.

(18) Goda, S.; Nikai, M.; Ito, M.; Hashizume, D.; Tamao, K.; Okazawa, A.; Kojima, N.; Fueno, H.; Tanaka, K.; Kobayashi, Y.; Matsuo, T. Synthesis and Magnetic Properties of Linear Two-coordinate Monomeric Diaryliron(II) Complexes Bearing Fused-ring Bulky "Rind" Groups. *Chem. Lett.* **2016**, *45* (6), 634−636.

(19) Merrill, W. A.; Stich, T. A.; Brynda, M.; Yeagle, G. J.; Fettinger, J. C.; De Hont, R.; Reiff, W. M.; Schulz, C. E.; Britt, R. D.; Power, P. P. Direct Spectroscopic Observation of Large Quenching of First-Order Orbital Angular Momentum with Bending in Monomeric, Two-Coordinate Fe(II) Primary Amido Complexes and the Profound Magnetic Effects of the Absence of Jahn− and Renner−Teller Distortions in Rigorously Linear Coordination. *J. Am. Chem. Soc.* **2009**, *131* (35), 12693−12702.

(20) Atanasov, M.; Zadrozny, J. M.; Long, J. R.; Neese, F. A theoretical analysis of chemical bonding, vibronic coupling, and magnetic anisotropy in linear iron(II) complexes with single-molecule magnet behavior. *Chem. Sci.* **2013**, *4* (1), 139−156.

(21) Meng, Y. S.; Mo, Z. B.; Wang, B. W.; Zhang, Y. Q.; Deng, L.; Gao, S. Observation of the single-ion magnet behavior of d^8 ions on two-coordinate Co(I)-NHC complexes. *Chem. Sci.* **2015**, *6* (12), 7156−7162.

(22) Poulten, R. C.; Page, M. J.; Algarra, A. G.; Le Roy, J. J.; López, I.; Carter, E.; Llobet, A.; Macgregor, S. A.; Mahon, M. F.; Murphy, D. M.; Murugesu, M.; Whittlesey, M. K. Synthesis, electronic structure, and magnetism of $[Ni(6-Mes)_2]^+$: a two-coordinate nickel(I) complex stabilized by bulky N-heterocyclic carbenes. *J. Am. Chem. Soc.* **2013**, *135* (37), 13640−13643.

(23) Iglesias, M.; Beetstra, D. J.; Knight, J. C.; Ooi, L.-L.; Stasch, A.; Coles, S.; Male, L.; Hursthouse, M. B.; Cavell, K. J.; Dervisi, A.; Fallis, I. A. Novel Expanded Ring N-Heterocyclic Carbenes: Free Carbenes, Silver Complexes, And Structures. *Organometallics* **2008**, *27* (13), 3279−3289.

(24) Boatner, L. A.; Abraham, M. M. Electron paramagnetic resonance from actinide elements. *Rep. Prog. Phys.* **1978**, *41* (1), 87−155.

(25) Mola, M.; Hill, S.; Goy, P.; Gross, M. Instrumentation for millimeter-wave magnetoelectrodynamic investigations of low-dimensional conductors and superconductors. *Rev. Sci. Instrum.* **2000**, *71* (1), 186−200.

(26) Takahashi, S.; Hill, S. Rotating cavity for high-field angle-dependent microwave spectroscopy of low-dimensional conductors and magnets. *Rev. Sci. Instrum.* **2005**, *76* (2), 023114.

(27) Ludwig, J.; Vasilyev, Y. B.; Mikhailov, N. N.; Poumirol, J. M.; Jiang, Z.; Vafek, O.; Smirnov, D. Cyclotron resonance of single-valley Dirac fermions in nearly gapless HgTe quantum wells. *Phys. Rev. B* **2014**, *89* (24), 241406.

(28) Neese, F. Software update: the ORCA program system, version 4.0. *Wiley Interdiscip. Rev.: Comput. Mol. Sci.* **2018**, *8* (1), e1327.

(29) Neese, F. The ORCA program system. *WIREs Comput. Mol. Sci.* **2012**, *2* (1), 73−78.

(30) Weigend, F.; Ahlrichs, R. Balanced basis sets of split valence, triple zeta valence and quadruple zeta valence quality for H to Rn: Design and assessment of accuracy. *Phys. Chem. Chem. Phys.* **2005**, *7* (18), 3297−3305.

(31) Aravena, D.; Neese, F.; Pantazis, D. A. Improved Segmented All-Electron Relativistically Contracted Basis Sets for the Lanthanides. *J. Chem. Theory Comput.* **2016**, *12* (3), 1148−1156.

(32) Jung, J.; Atanasov, M.; Neese, F. Ab Initio Ligand-Field Theory Analysis and Covalency Trends in Actinide and Lanthanide Free Ions and Octahedral Complexes. *Inorg. Chem.* **2017**, *56* (15), 8802−8816.

(33) Rieger, P. H. Electron paramagnetic resonance studies of low-spin d^5 transition metal complexes. *Coord. Chem. Rev.* **1994**, *135−136*, 203−286.

(34) McGarvey, B. R. Survey of ligand field parameters of strong field d^5 complexes obtained from the g matrix. *Coord. Chem. Rev.* **1998**, *170* (1), 75−92.

(35) Krishnamurthy, R.; Schaap, W. B. Computing ligand field potentials and relative energies of d orbitals: A simple general approach. *J. Chem. Educ.* **1969**, *46* (12), 799.

(36) Wagner, C. L.; Tao, L.; Fettinger, J. C.; Britt, R. D.; Power, P. P. Two-coordinate, late first-row transition metal amido derivatives of the bulky ligand -N(SiPr$^i_3$)Dipp (Dipp = 2,6-diisopropylphenyl): effects of the ligand on the stability of two-coordinate copper(II) complexes. *Inorg. Chem.* **2019**, *58* (13), 8793−8799.

(37) Samuel, P. P.; Mondal, K. C.; Roesky, H. W.; Hermann, M.; Frenking, G.; Demeshko, S.; Meyer, F.; Stückl, A. C.; Christian, J. H.; Dalal, N. S.; Ungur, L.; Chibotaru, L. F.; Pröpper, K.; Meents, A.; Dittrich, B. Synthesis and characterization of a two-coordinate manganese complex and its reaction with molecular hydrogen at room temperature. *Angew. Chemie Int. Ed.* **2013**, *52* (45), 11817−11821.

(38) Reta, D.; Chilton, N. F. Uncertainty estimates for magnetic relaxation times and magnetic relaxation parameters. *Phys. Chem. Chem. Phys.* **2019**, *21* (42), 23567−23575.

(39) Lunghi, A.; Totti, F.; Sessoli, R.; Sanvito, S. The role of anharmonic phonons in under-barrier spin relaxation of single molecule magnets. *Nat. Commun.* **2017**, *8* (1), 14620.

(40) Lunghi, A.; Totti, F.; Sanvito, S.; Sessoli, R. Intra-molecular origin of the spin-phonon coupling in slow-relaxing molecular magnets. *Chem. Sci.* **2017**, *8* (9), 6051−6059.

(41) Lunghi, A.; Sanvito, S. How do phonons relax molecular spins? *Sci. Adv.* **2019**, *5* (9), eaax7163.

(42) Albino, A.; Benci, S.; Tesi, L.; Atzori, M.; Torre, R.; Sanvito, S.; Sessoli, R.; Lunghi, A. First-principles investigation of spin−phonon coupling in vanadium-based molecular spin quantum bits. *Inorg. Chem.* **2019**, *58* (15), 10260−10268.

(43) Briganti, M.; Santanni, F.; Tesi, L.; Totti, F.; Sessoli, R.; Lunghi, A. A Complete Ab Initio View of Orbach and Raman Spin−Lattice Relaxation in a Dysprosium Coordination Compound. *J. Am. Chem. Soc.* **2021**, *143* (34), 13633−13645.